Metallurgical and Materials Transactions A 51 (2020) 1395-1401

Devitrification of mechanically alloyed Fe-Nb system: Mössbauer study of the intermetallic phases

A.F. Manchón-Gordón[1], P. Svec[2], J.J. Ipus[1], M. Kowalczyk[3], J.S. Blázquez[*1], C.F. Conde[1], A. Conde[1], P. Svec Sr.[2], T. Kulik[3]

[1]*Dpto. Física de la Materia Condensada, ICMSE-CSIC, Universidad de Sevilla, P.O. Box 1065, 41080 Sevilla, Spain*
[2]*Institute of Physics. Slovak Academy of Sciences. Dúbravská cesta 9, 845 11 Bratislava 45, Slovak Republic.*
[3] *Faculty of Materials Science and Engineering, Warsaw University of Technology, 141 Wołoska st., 02-507 Warsaw, Poland*
[*]*The corresponding author e-mail:* jsebas@us.es

ABSTRACT: Intermetallic phases in the Fe-Nb system have been obtained as products of the devitrification of a homogeneous amorphous $Fe_{70}Nb_{30}$ alloy prepared by mechanical alloying. Besides Fe_2Nb Laves and Fe_7Nb_6 intermetallic phases, α-Fe phase has been detected by X-ray diffraction (XRD). Hyperfine parameters for both Fe_2Nb and Fe_7Nb_6 intermetallics have been obtained from Mössbauer spectroscopy in correlation with phase identification from XRD results. Thermomagnetic measurements show changes in the Curie temperatures of the amorphous and Fe_2Nb phases during the crystallization, due to compositional variations related to the developing of the α-Fe phase. Kinetics of the crystallization process has been analyzed using the classical Johnson-Mehl-Avrami-Kolmogorov kinetic theory in both isothermal and non-isothermal regimes.

KEYWORDS: Fe-Nb intermetallics, amorphous and nanocrystalline alloys, Mössbauer spectroscopy, crystallization kinetics.

1. INTRODUCTION

Fe-Nb systems have received a particular interest in the research community essentially due to their wide range of different applications in industry, mainly as special stainless steels[1-4] and as soft magnets[5,6]. Indeed, the presence of Nb in the Fe matrix limits the formation of α-Fe grains to the nanometric scale, improving the mechanical properties (through solid solution and/or precipitation strengthening[1,2]) and the magnetic softness (through averaging out the magnetocrystalline anisotropy[7]).

In spite of the interest on this system, there are some discrepancies in the literature on the complete Fe-Nb phase diagram, particularly on the melt and the homogeneity ranges of the intermetallic phases[8-10]. In fact, while a previous Fe-Nb phase diagram[11] showed four intermetallics (including a possible high temperature phase at 90 at.% Nb), recent results indicate the existence of only two intermetallic phases, the hexagonal Fe_2Nb and the trigonal Fe_7Nb_6 phases[8].

Many techniques have been used to produce Fe-Nb alloys. However, the poor solubility of niobium in the iron lattice (Fe-Nb mixing enthalpy -16 kJ/mol[12]) limits the production of homogenous Fe-Nb systems by melting methods to concentrations higher than 33 at.% Nb[13], due to the large difference between the melting temperatures of these elements (1811 and 2750 K for Fe and Nb, respectively[8]). Therefore, the production of samples out of the eutectic compositions requires other ways, such as mechanical alloying. This method often produces non-equilibrium solid solutions and amorphous phases[14-16]. Consequently, additional thermal treatments are necessary to develop stable crystalline phases. In this sense, the combination of X-ray diffraction (XRD) and Mössbauer spectroscopy (MS) techniques in iron-based systems allows studying in detail the final products of the crystallization process[17,18].

Concerning the devitrification process, crystallization kinetics can be characterized by Johnson and Mehl[19], Avrami[20] and Kolmogorov[21] classical crystallization theory (JMAK theory). Although JMAK theory was developed to be applied to isothermal polymorphic transformations, it has been successfully extended to transformations implying compositional changes[22,23] and to non-isothermal processes[24-29]. Compared to isothermal experiments, non-isothermal processes have the advantages of an easier operation, lower time cost and higher signal-to-noise ratio[28].

In this work, an amorphous Fe alloy with 30 at.% Nb has been synthesized by means of mechanical alloying in order to obtain a homogeneous sample. Different thermal treatments have been applied in order to develop stable intermetallic Fe-Nb phases. The products of the crystallization process have been studied by X-ray diffraction (XRD), Mössbauer spectroscopy (MS) and magnetometry. JMAK theory has been used to describe the crystallization process for non-isothermal and isothermal regimes.

2. EXPERIMENTAL

Amorphous alloy with $Fe_{70}Nb_{30}$ at.% composition was prepared by high energy ball milling, starting from high purity elemental powders of iron and niobium (>99.9 %). The milling was carried out for 50 hours at 350 rpm in a planetary ball mill Fritsch Pulverisette Vario 4. Further milling parameters and a detailed microstructural evolution of the sample with milling time can be found elsewhere[16].

Differential thermal analysis (DTA) was carried out in a Perkin-Elmer DTA7 unit under Ar flow for both isothermal and non-isothermal experiments. Different heating rates (β=5, 10, 20, 40 and 60 K/min) were used for non-isothermal treatments up to 1300 K without evidencing any changes (see supplementary material). In order to follow the

progress of the transformations, heating at 10 K/min up to different temperatures (from 908 to 1300 K) was also performed. In the case of isothermal experiments, the amorphous sample was annealed for 5 hours at 954 K, 10 K below the onset temperature obtained for β=10 K/min (see Fig. 1a). The corresponding baselines were obtained repeating the same treatment after the complete crystallization of the sample.

XRD patterns were recorded in a Bruker D8 Advance diffractometer (Cr-Kα, λ=2.28970 Å) in a Bragg-Brentano geometry. The local environment of Fe atoms was analyzed at room temperature by Mössbauer spectrometry in transmission geometry using a ^{57}Co(Rh) source. Values of the hyperfine parameters were obtained by fitting the measured spectra with the NORMOS program[30] and the isomer shift (IS) was quoted relative to that of an α-Fe foil at room temperature.

Magnetization measurements were performed in a vibrating sample magnetometer (standard option of a Quantum Design Physical Properties Measurement System, PPMS) applying a magnetic field of 100 Oe. Curie temperatures T_C have been determined by identifying the temperature at which the temperature derivative of magnetization shows a minimum.

3. RESULTS and DISCUSSION

3.1. Characterization of crystallization products

Figure 1a shows the non-isothermal DTA plot taken at 10 K/min for the as-milled amorphous sample. All the features found in the curve vanish in a second heating, which was used as the corresponding baseline. Deviations from baseline at lower temperatures are ascribed to relaxation phenomena. A well-defined exothermic peak can be observed around 950 K, corresponding to the crystallization of the amorphous phase. The measured peak shape in Fig. 1a suggests that at least two transformations are taking

place. However, no experimental deconvolution could be obtained in the heating rate from 5 to 60 K/min (see figure 1b). A second and weaker peak is observed at ~1200 K in Fig. 1a. The effective value of the activation energy E_a=2.48±0.07 eV/at, corresponding to the first peak temperature, has been calculated by Kissinger's method[31] (see inset of Fig. 1b). This value is similar to that reported by El-Eskandarany et al.[32] for the crystallization of the amorphous $Fe_{52}Nb_{48}$ alloy powder obtained by mechanical alloying.

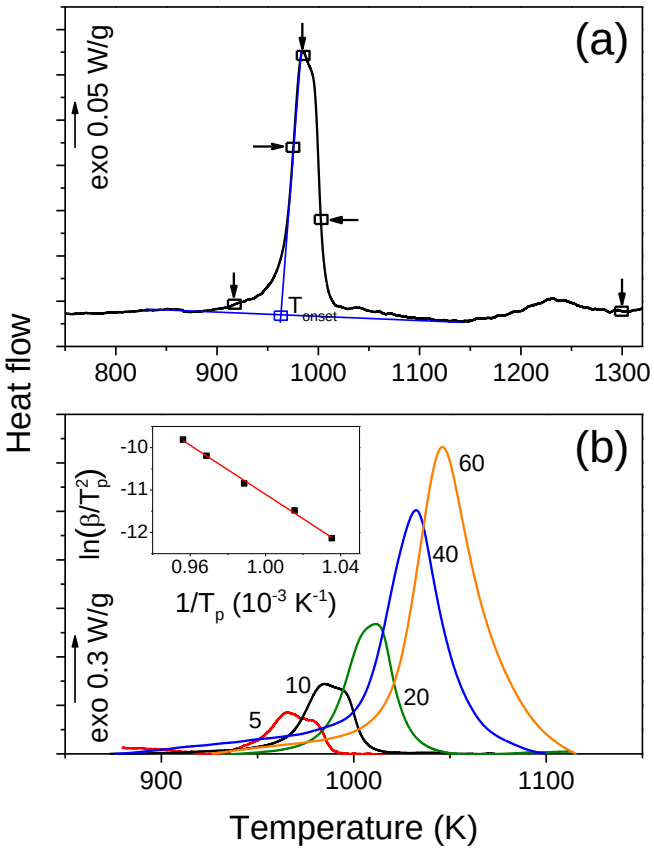

Figure 1. (a) Non-isothermal DTA scan at 10 K/min for the as-milled sample. Arrows indicate the temperatures up to which different samples have been heated. The onset temperature is indicated. (b) Non-isothermal DTA scans for as-milled sample at the different indicated heating rates (in K/min) in the region of the first DTA exotherm. The inset shows the Kissinger's plot.

Figure 2 shows the XRD patterns of as-milled sample and of those samples after heating at 10K/min up to the indicated temperatures to evidence the formation of the different crystalline phases. The as-milled powders only show a broad halo distinctive of an amorphous phase. This broad halo is the only feature observed in the patterns collected for samples heated up to 907 K. Above this temperature, several diffraction peaks appear superimposed to the amorphous halo, corresponding to three phases: hcp Fe_2Nb (after heating up to 968 K, with space group $P6_3/mmc$), bcc-Fe (after heating up to 1003 K, with space group Im3m) and trigonal Fe_7Nb_6 (space group R-3m, after heating up to 1273 K).

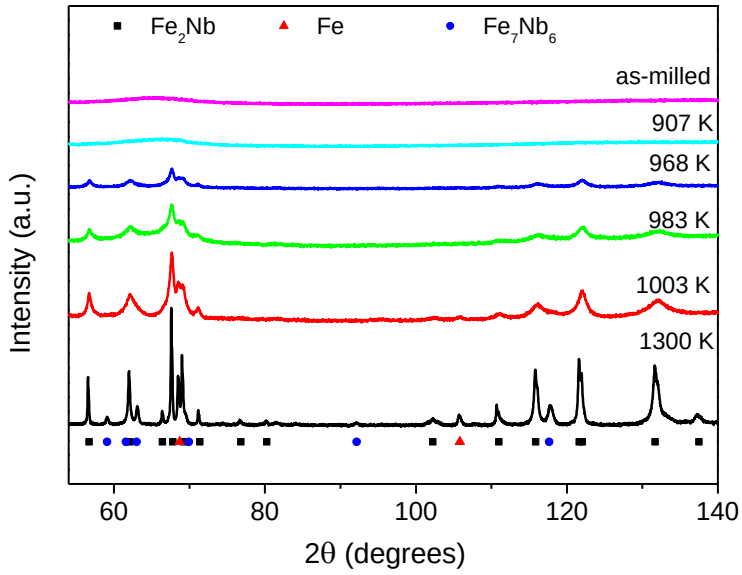

Figure 2. XRD patterns taken at room temperature of as-milled amorphous powders and of samples heated at 10 K/min up to the indicated temperatures. These temperatures correspond to those indicated by arrows in Figure 1a.

Figure 3 shows the room temperature Mössbauer spectra of as-milled and heat treated samples up to the different indicated temperatures at β=10 K/min. A quadrupolar distribution has been used to describe the paramagnetic contribution, assigned to the amorphous phase. The quadrupolar distribution is the unique contribution that exhibits

the alloy heated up to 907 K, in agreement with the XRD results, showing only an amorphous phase. Above this temperature, MS spectra show a decrease of the relative area of the quadrupolar distribution along with the appearance of a doublet, indicating the migration of Fe atoms to an ordered structure which corresponds to the Fe_2Nb intermetallic detected by XRD. After heating up to 983 K, besides the quadrupolar distribution and the doublet, a sextet appears with an hyperfine magnetic field of 32.84±0.09 T corresponding to the α-Fe phase, detected also by XRD but after heating up to 1003 K. In fact, MS is a more sensitive technique than XRD in order to detect small fractions of Fe-phases when paramagnetic and ferromagnetic phases coexist[16]. After heating up to 1300 K, the alloy is totally crystalline, evidenced by the absence of any quadrupolar distribution. A new doublet was used to fit the spectrum showing the appearance of a new ordered phase, in agreement with the detection of Fe_7Nb_6 in the corresponding XRD patterns. The presence of doublets is frequently reported in the Mössbauer spectra of Fe-Nb alloys[32-34].

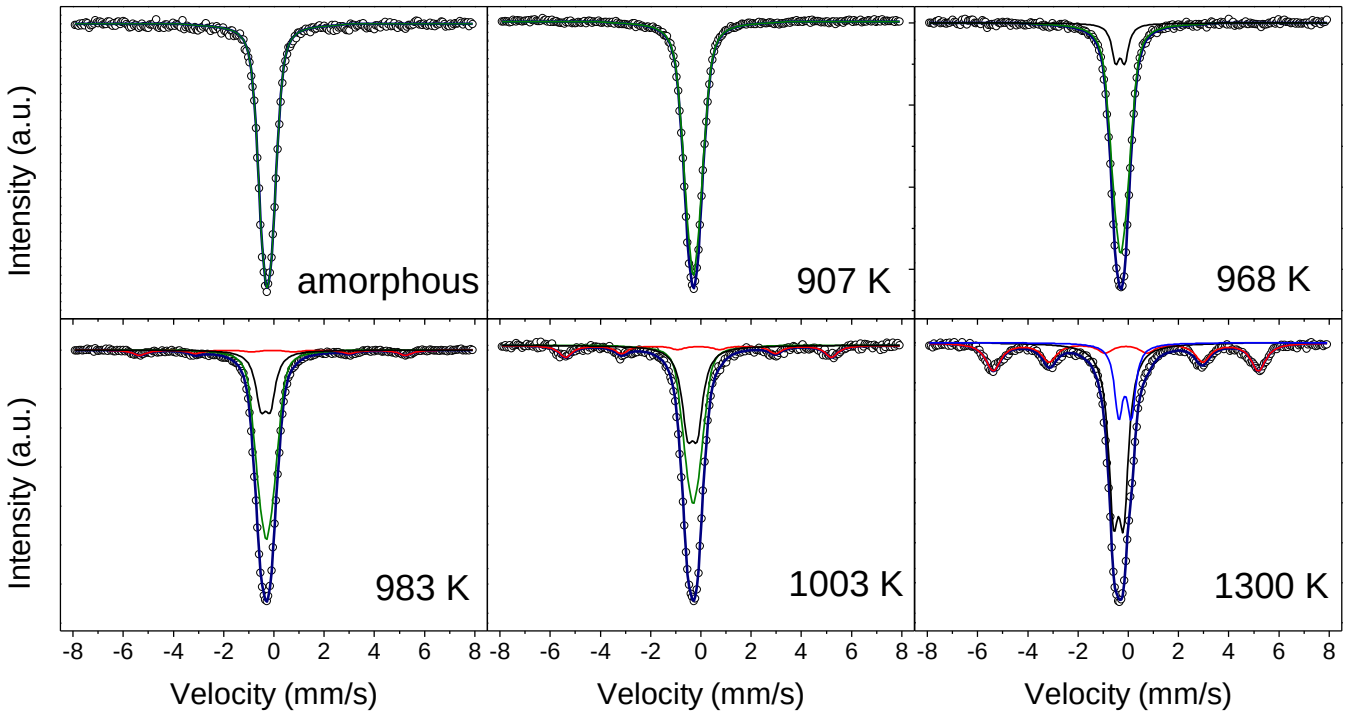

Figure 3. Experimental Mössbauer spectra taken at room temperature (symbols) and model fitting (lines) of as-milled and heat treated samples at 10 K/min up to the indicated temperatures. These temperatures correspond to those indicated by arrows in Figure 1a. Green, black, red and blue subspectra correspond to Fe atoms in the amorphous, Fe_2Nb, α-Fe and Fe_7Nb_6 phases, respectively.

Figure 4a shows the evolution of the fraction areas of different contributions to Mössbauer spectra as a function of the final heating temperature at β=10 K/min (values at 300 K correspond to the as-milled sample with 100% amorphous phase). Doublet 1 (ascribed to Fe sites in Fe_2Nb) is the first contribution detected and its fraction shows a continuous increase up to ~50 % as the final heating temperature increases. The ferromagnetic site (ascribed to α-Fe) is clearly detected after heating up to 983 K. On the other hand, doublet 2 (ascribed to Fe sites in Fe_7Nb_6) is not detected until the sample is heated up to 1300 K, when the area fraction of this contribution reaches ~20 %. The different fraction areas of the samples are practically independent of the heating rate, as is shown in Fig. 4b. Only in the case of β=5 K/min, the decrease of the doublet 1 fraction is compensated by an increase of the fraction of the ferromagnetic site and the doublet 2.

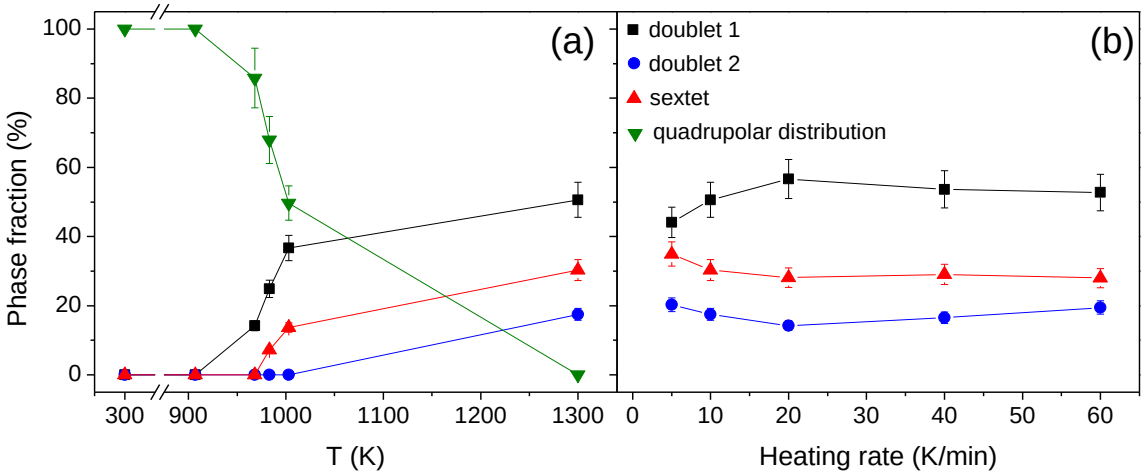

Figure 4. Evolution of the phase fraction obtained by MS as a function of a) the maximum heating temperature reached at 10 K/min and b) the heating rate up to 1300 K. Lines are guides to the eye.

The fitted hyperfine values for doublet 1, attributed to the Fe_2Nb crystalline phase, are a quadrupole splitting Q=0.40±0.02 mm/s and an isomer shift δ=-0.30±0.01 mm/s. Doublet 2, assigned to the Fe_7Nb_6 intermetallic, exhibits a Q=0.45±0.07 mm/s and δ=-0.03±0.04 mm/s. These values and the average values found for the as-milled amorphous sample are shown in Table 1 and can be compared to those reported in the literature for samples prepared by different methods[35-38].

Table 1. Hyperfine parameters of as-milled amorphous alloy and of sample heated up to 1300 K along with those of other FeNb alloys from the literature. % is the relative contribution of the component, δ is the isomer shift relative to α-Fe, Q is the quadrupole splitting and B_{hf} the hyperfine field magnetic field.

Technique	**Component**	**%**	**δ (mm/s)**	**Q (mm/s)**	**B_{hf} (T)**	**Ref.**
Mechanical alloying	Quadrupolar distribution (amorphous)	100	-0.17±0.01	0.32±0.01	-	This work
Mechanical alloying + heating treatment	Doublet1 (Fe_2Nb)	47	-0.30±0.01	0.40±0.02	-	This work
	Doublet2 (Fe_7Nb_6)	23	-0.03±0.04	0.45±0.07	-	
	Sextet (α-Fe)	30	0.004±0.003	0	32.84±0.09	
Arc-melting + heating treatment	Doublet1	-	-0.258	0.310	-	[35]
	Doublet2	-	-0.228	0.232	-	
Mechanical alloying + heating treatment	Doublet1	62	-0.19±0.01	0.34±0.05	-	[36]
	Doublet2	18	0.02±0.05	0.41±0.05	-	
	Sextet	20	0.00±0.05	-0.04±0.05	33.7±0.2	
Arc-melting	Doublet1	15	-0.24±0.03	0.37±0.04	-	[37]
	Sextet	85	0.004±0.002	-	32.63±0.02	
Magnetron sputtering	Doublet1	10	-0.3±0.1	0.4±0.1	-	[38]
	Sextet	65	-	-	33.1	

Although values reported in the literature are similar, they are dispersed between those here assigned to the amorphous phase and those here assigned to the intermetallics. In the present study, the combination of the MS with XRD results of partially crystallized samples allowed us to unambiguously assign the hyperfine parameters to each of the phases detected. In fact, two doublets have been also detected by Raposo et al.[35] for

bulk alloys produced by arc-melting. They found Q=0.31 mm/s and δ=-0.258 mm/s for Fe_2Nb and Q=0.232 mm/s and δ=-0.228 mm/s for Fe_7Nb_6. Although they reported clearly different values for Fe_7Nb_6 intermetallic, it is worth mentioning that this phase was not detected in their XRD patterns. In the work of Velez et al.[36], the Fe_7Nb_6 phase was not detected from X-ray patterns but they reported two doublets to fit the Mössbauer spectra. However, they attributed the values of the second one (Q=0.41$\pm$0.05 mm/s and δ=0.02$\pm$0.01), which are close to those assigned in our study to Fe_7Nb_6, to "the contribution of the hcp amorphous grain boundaries and to the incoherent surface of these grains".

Figure 5 shows the temperature dependence of magnetization at 100 Oe during cooling samples previously heated up to the indicated temperatures. The as-milled amorphous sample heated up to 908 K undergoes magnetic transition from paramagnetic to ferromagnetic phase at T_C=34 K. After heating up to 968 K two magnetic transitions can be observed in agreement with the presence of amorphous and Fe_2Nb phases detected from XRD patterns. Sample heated up to 973 K shows the same features. The first transition is still attributed to the T_C of the amorphous phase, that changes from 34 to 84 K. The second transition corresponds to the Curie temperature of the Fe_2Nb phase, which changes from 177 to 189 K for the sample heated up to 968 and 973 K, respectively. These changes in the T_C can be understood if the compositional changes of the amorphous phase due to the formation of the intermetallic phase are considered.

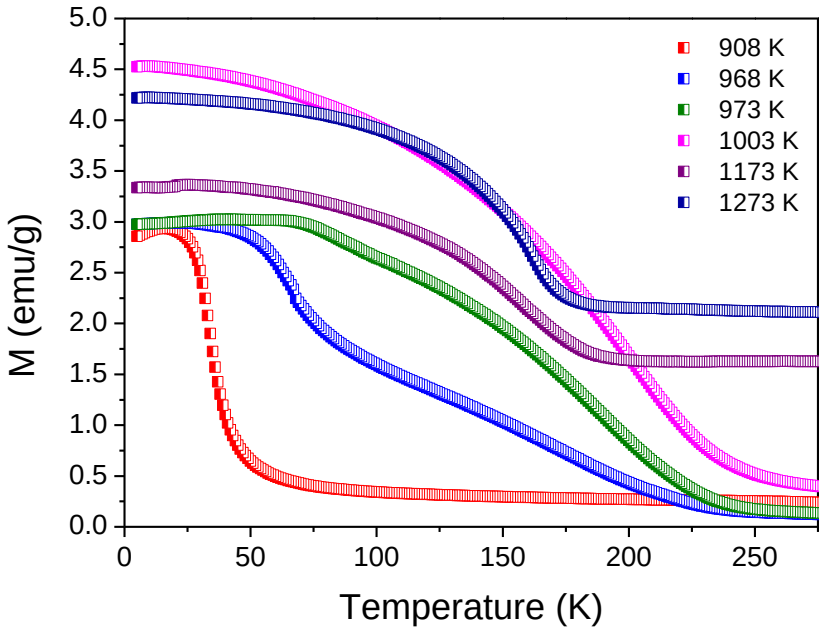

Figure 5. M(T) curves under a low magnetic field of 100 Oe for samples previously heated at 10K/min up to the indicated temperatures.

For samples heated up to 1003 K, the contribution of the amorphous phase disappears and only a magnetic transition at T_C=199 K can be observed, associated to the Fe_2Nb intermetallic phase. Above this temperature, the magnetization does not go to zero above the T_C of the Fe_2Nb phase because of the developing of the α-Fe phase, the amount of which increases as the temperature of the heating treatment increases, in good agreement with the XRD results. The final Curie temperature of the Fe_2Nb phase is 162 K. This decrease of T_C corresponds to Fe depletion in the intermetallic phase due to the developing of the α-Fe phase.

3.2. Crystallization kinetics

In order to obtain the local values of the Avrami exponents as a function of the transformed fraction, $n(X)$, DTA isothermal experiments were performed annealing the

as-milled sample for 5 hours at 954 K (10 K below the onset temperature obtained for β=10 K/min). Avrami exponent can be obtained from JMAK equation as:

$$n = \frac{d(\ln[-\ln(1-X)])}{d(\ln(t-t_0))} \quad (1)$$

where t_0 is the induction time. A non-isothermal scan after the isothermal one did not show any exothermic peak, indicating that the transformation was completed during the isothermal treatment. This agrees with the detection of the three phases in XRD patterns of samples after the isothermal treatment (see figure 6a).

The transformed fraction X has been approximated to the normalized transformed enthalpy, $X = \Delta H_{iso}(t)/\Delta H_{total}^{iso}$, where $\Delta H_{iso}(t)$ is the enthalpy at a time t and is obtained from integrating the isothermal DTA peak up to this time t, and ΔH_{total}^{iso}=40 J/g is the total enthalpy of the crystallization process. It is worth noticing that for very small and very high X values, the effects of errors in baseline are more important.

Non-isothermal kinetics was also studied. In this case, a direct approach to non-isothermal processes of the JMAK theory has been applied[28]. This approach allows us to obtain the $n(X)$ values as:

$$\frac{d(\ln[-\ln(1-X)])}{d\left(\ln\left[\frac{T-T_0}{\beta}\right]\right)} = n\left\{1 + \frac{E_a}{RT}\left(1 - \frac{T_0}{T}\right)\right\} \quad (2)$$

where E_a is the activation energy, R is the ideal gas constant and T_0=$T_p/2$, being T_p the peak temperature, an effective onset temperature that minimizes the error of the used approximation[39]. The transformed fraction has been approximated to the normalized transformed enthalpy, $X = \Delta H(T)/\Delta H_{total}^{non-iso}$, where $\Delta H(T)$ is the enthalpy developed up to temperature T and $\Delta H_{total}^{non-iso}$=59 J/g is the enthalpy of the complete crystallization process. This larger enthalpy value with respect to that of isothermal

treatment could be understood as a more developed crystallization process (grain growth and coalescence) in agreement with the XRD patterns shown in Figure 6a.

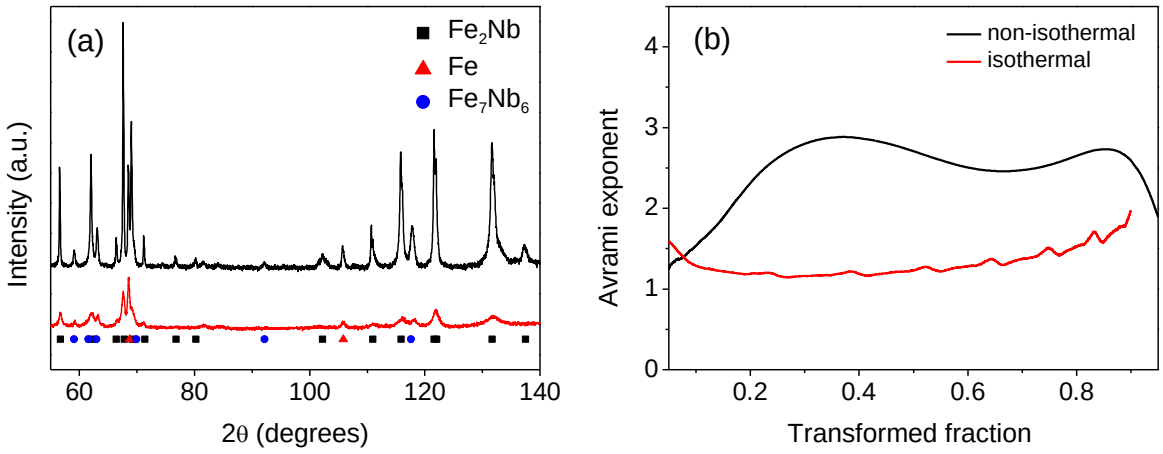

Figure 6. a) XRD patterns after non-isothermal treatment (heating at 10 K/min up to the end of the first DTA exotherm; T=1300 K) and isothermal one (5 h at 954 K). b) Experimental local Avrami exponents as a function of transformed fraction of the crystallization process for $Fe_{70}Nb_{30}$ amorphous alloys heated at β=10 K/min and in isothermal regime (T=954 K), respectively.

Figure 6b shows the local Avrami exponent as a function of the transformed fraction X calculated using Eq. 1 for isothermal treatment (T_{iso}=954 K) and Eq. 2 for non-isothermal one at β=10 K/min for the first exothermic peak. XRD and MS show that independent transformations simultaneously occur during the crystallization process (formation of the Fe_2Nb, α-Fe and Fe_7Nb_6 crystalline phases). However, the first phase to appear is Fe_2Nb, which is also the main phase. Taking into account that after heating up to 1003 K ~90 % of the enthalpy of the process is completed and besides Fe_2Nb peaks, only traces of α-Fe phase are observed, kinetic results should correspond mainly to the crystallization of Fe_2Nb intermetallic.

The obtained values, n_{iso}~1, for the isothermal case are typical for nanocrystallization processes for which growth is severely impinged. In the case of the non-isothermal

experiments, the Avrami exponent in the range $0.2<X<0.7$ is $n=2.65\pm0.16$. This can be interpreted as a constant nucleation rate and a three dimensional diffusion controlled growth (mainly formation of hexagonal Fe_2Nb Laves phase). Therefore, the differences between isothermal and non-isothermal kinetic results could be ascribed to a stronger impingement in the growth of the Fe_2Nb crystals in the isothermal regime. In fact, the isothermal growth process occurs at a much lower temperature than for non-isothermal treatments. This agrees with a much broader XRD diffraction maxima for isothermally annealed samples than for non-isothermal treated ones (Fig. 6a) indicating a clearly smaller crystallite size of the isothermally treated samples.

4. Summary and conclusions

Mechanical alloying allows us to obtain homogeneous Nb-30 at.% Fe amorphous alloy as a precursor system from which different iso- and non-isothermal treatments have been applied to develop crystalline stable phases. The products of the crystallization process have been studied by X-ray diffraction and Mössbauer spectroscopy as a function of both the final heating temperature and the heating rates. X-ray patterns clearly provide evidence of the formation of two intermetallics: Fe_2Nb and Fe_7Nb_6, as well as bcc-Fe crystalline phase. Mössbauer spectra are consistent with the XRD results, showing the existence of three different kinds of local environments and allowing us to obtain the hyperfine parameters of the intermetallic phases. The decomposition of the paramagnetic contribution into two doublets indicates a migration of atoms from the amorphous phase to ordered structures, ascribed to intermetallic phases. The sequence in which they are detected from XRD allows us a clear assignment of the hyperfine parameters to each intermetallic phase. Temperature dependent magnetization curves

show the evolution of the Curie temperatures of the amorphous and Fe_2Nb phases during the crystallization, as well as the developing of the bcc-Fe crystalline phase.

JMAK theory has been used to describe the crystallization process in both isothermal and non-isothermal regimes. A stronger growth impingement in the isothermal regime can explain the lower Avrami exponent found with respect to those obtained for non-isothermal treatments.

Acknowledgements

This work was supported by AEI/FEDER-UE (Project MAT 2016-77265-R) and the PAI of the Regional Government of Andalucía. Support of the project APVV-15-0621 is also acknowledged. A.F. Manchón-Gordón acknowledges his contract to the VPPI-US of the University of Sevilla.

References

1 N. Fujita, K. Ohmura, A. Yamamoto: *Mater. Sci. Eng., A.* 2003, vol. 351, pp. 272-281.
2 G.M. Sim, J.C. Ahn, S.C. Hong, K.J. Lee, K. S. Lee: *Mater. Sci. Eng., A.* 2005, vol. 396, pp. 159-165.
3 A. Malfliet, W. Van den Broek, F. Chassagne, J.D. Mithieux, B. Blanpain, P. Wollants: *J. Alloy Comp.* 2011, vol. 509, pp. 9583-9588.
4 Y. Kang, W.M. Mao, Y.J. Chen, J. Jing, M. Cheng: *Mater. Sci. Eng., A.* 2016, vol. 677, pp. 453-464.
5 M.E. McHenry, M.A. Willard, D.E. Laughlin: *Prog. Mater. Sci.* 1999, vol. 44, pp. 291-433.
6 L.E. Zamora, G.A.P. Alcazar, J.A. Tabares, J.D. Betancur, F.R. Sives, J. Jaen, J.M. Greneche, J.F. Marco, J.M. Gonzalez: *J. Phys. D: Appl. Phys.* 2008, vol. 41, p. 155010.
7 G. Herzer: *Scr. Metall. Mater.* 1995, vol. 33, pp. 1741-1756.
8 S. Voss, M. Palm, F. Stein, D. Raabe: *J. Phase Equilib. Diffus.* 2011, vol. 32, pp. 97-104.
9 K.W. Li, X.B. Wang, S.M. Li, W.X. Wang, S.P. Chen, D.Q. Gong, J.L. Cui: *High. Temp. Mater. Processes (Berlin, Ger.)* 2015, vol. 34, pp. 479-485.
10 C.G. Schon, J.A.S. Tenorio: *Intermetallics* 1996, vol. 4, pp. 211-216.
11 H.J. Goldschmidt: *Research (London)* 1957, vol. 10, pp. 289-291.
12 A. Takeuchi, A. Inoue: *Mater. Trans., JIM* 2000, vol. 41, pp. 1372-1378.
13 E.P. Abrahamson, S.L. Lopata: *Trans. Metall. Soc. AIME* 1966, vol. 236, pp. 76-87.
14 J.J. Ipus, J.S. Blázquez, V. Franco, A. Conde, L.F. Kiss: *Intermetallics* 2010, vol. 18, pp. 565-568.
15 J.S. Blázquez, J.J. Ipus, S. Lozano-Perez, A. Conde: *JOM* 2013, vol. 65, pp. 870-882.
16 A.F. Manchón-Gordón, J.J. Ipus, J.S.; Blázquez, C.F. Conde, A. Conde: *J. Non-Cryst. Solids* 2018, vol. 494, pp. 78-85.
17 J. Balogh, L. Bujdoso, D. Kaptas, T. Kemeny, I. Vincze, S. Szabo, D.L. Beke: *Phys. Rev. B* 2000, vol. 61, pp. 4109-4116.
18 J.S. Blázquez, J.J. Ipus, V. Franco, C.F. Conde, A. Conde: *J. Alloy Comp.* 2014, vol. 610, pp. 92-99.
19 W.A. Johnson, R.F. Mehl: *Tech. Publ. - Am. Inst. Min. Metall. Eng.* 1939, *135*, 416–442.
20 M. Avrami: *J. Chem. Phys.* 1941, vol. 9, pp. 177-184.
21 A.N. Kolmogorov, *Bull. Russ. Acad. Sci.* 1937, vol. 1, pp. 355–359.
22 P. Bruna, D. Crespo, R. Gonzalez-Cinca, E. Pineda: *J. Appl. Phys.* 2006, vol. 100, p. 054907.
23 J.S. Blázquez, M. Millán, C.F. Conde, A. Conde: *J. Alloy Comp.* 2010, vol. 505, pp. 91-95.
24 T. Ozawa, *Polymer* 1971, vol. 12, pp. 150-158.
25 K. Nakamura, T. Watanabe, K. Katayama: *J. Appl. Polym. Sci.* 1972, vol. 16, pp. 1077-1091.
26 K. Nakamura, T. Watanabe, T. Amano: *J. Appl. Polym. Sci.* 1974, vol. 18, pp. 615-623.
27 M.J. Starink, A.M. Zahra: *Thermochim. Acta* 1997, vol. 298, pp. 179-189.
28 J.S. Blázquez, C.F. Conde, A. Conde: *Acta Mater.* 2005, vol. 53, pp. 2305-2311.
29 J. Torrens-Serra, P. Bruna, S. Roth, J. Rodriguez-Viejo, M.T. Clavaguera-Mora: *J. Alloy Comp.* 2010, vol. 496, pp. 202-207.
30 R.A. Brand, J. Lauer, D.M. Herlach: *J. Phys. D: Appl. Phys.* 1983, vol. 13, pp. 675-683.
31 H.E. Kissinger: *Anal. Chem.* 1957, vol. 29, pp. 1702-1706.
32 M.S. El-Eskandarany, A.A. Bahgat, N.S. Gomaa, N.A. Eissa: *J. Alloy Comp.* 1999, vol. 290, pp. 181-190.
33 E. Jartych, D. Oleszak, J.K. Zurawicz: *Hyperfine Interact.* 2001, vol. 136, pp.25-33.
34 G.Y. Velez, G.A. Perez Alcazar, L.E. Zamora: *J. Magn. Magn. Mater.* 2014, vol. 354, pp. 333-335.
35 M.T. Raposo, J.D. Ardisson, A.I.C. Persiano, R.A. Mansur: *Hyperfine Interact.* 1994, vol. 83, pp. 235-238.

36 G.Y. Velez, G.A. Perez Alcazar, L.E. Zamora, J.A. Tabares: *J. Supercond. Novel Magn.* 2014, vol. 27, pp. 1279-1283.
37 A. Blachowski, K. Ruebenbauer, J. Zukrowski: *Phys. Status Solidi* B 2005, vol. 242, pp. 3201-3208.
38 M.J.M. Pires, W.A.A. Macedo, L.P. Cavalcanti, A.M.G. Carvalho, *J. Phys. Chem. Solids* 2015, vol. 86, pp. 36-41.
39 J.S. Blázquez, J.M. Borrego, C.F. Conde, A. Conde, S. Lozano-Perez: *J. Alloy Comp.* 2012, vol. 544, pp. 73-81.